A GRAPHICAL-NUMERICAL PREDICTION OF THE 1000-MB SURFACE WITH NON-ADIABATIC WARMING

YEH-CHUN WANG

A GRAPHICAL-NUMERICAL PREDICTION OF THE 1000-MB SURFACE WITH NON-ADIABATIC WARMING

* * * *

Yeh-Chun Wang

A GRAPHICAL-NUMERICAL PREDICTION OF THE 1000-MB SURFACE WITH NON-ADIABATIC WARMING

by

Yeh-Chun Wang
//
Lieutenant Commander

The Republic of China Navy

Submitted in partial fulfillment of
the requirements for the degree of

MASTER OF SCIENCE

IN

METEOROLOGY

United States Naval Postgraduate School
Monterey, California
United States of America

1 9 5 9

A GRAPHICAL-NUMERICAL PREDICTION OF THE 1000-MB SURFACE WITH NON-ADIABATIC WARMING

by

Yeh-Chun Wang

This work is accepted as fulfilling

the thesis requirements for the degree of

MASTER OF SCIENCE

IN

METEOROLOGY

from the

United States Naval Postgraduate School

ABSTRACT

A two-level graphical-numerical prediction model is extended so as to incorporate some orographical and non-adiabatic warming or cooling effects in a manner such that almost no extra work is added.

The model is applied to several cases where non-adiabatic heat exchanges are pronounced. The resulting prognoses show a material improvement over a similar model which omits the non-adiabatic influence.

TABLE OF CONTENTS

LIST OF ILLUSTRATIONS

1. Introduction

It is a well-known fact that during the winter season cold cP air flowing out from continent over the warm ocean surface will acquire heat energy from below so that the lower layers of the atmosphere are warmed. As Craddock [1] measured in the case when the arctic air flowed out from Iceland to the British Isles, the heating rate may be as large as 65/ly per hour and in the course of a day the 1000-500 mb layer thickness could increase approximately 800 feet. Hence, in such cases, an appreciable error will be produced in the results of those numerical prediction models which assume that the air motion is adiabatic. Several techniques have been introduced to eliminate this non-adiabatic error; Reed [5] has incorporated Burke's semi-empirical treatment for the air mass transformation cP-mP into a graphical model of numerical prognosis. His results show considerable improvement over a model omitting the non-adiabatic heating.

In the present investigation, the non-adiabatic heating (or cooling) is approximated in a rather crude but extremely simple manner. As a result there is no additional work when non-adiabatic heating and the orographic influences [3] are included.

2. Development of the prediction equation

The basic vorticity equation in the (x,y,p,t) coordinates takes the form

$$\frac{D(\zeta + f)}{Dt} = -f\nabla\cdot V \tag{1}$$

where $\frac{D}{Dt}$ is the individual rate-of-change operator following the isobaric projection of the three-dimensional motion,

ζ the relative vorticity,

f coriolis force,

∇ del operator.

Both ζ and ∇ refer to values measured on an isobaric surface.

In Eq. (1) the terms involving the vortex tube and vertical advection of vorticity have been neglected, and also the term $-\zeta\nabla\cdot V$ [6].

Expanding the left side of Eq. (1),

$$\frac{\partial}{\partial t}(\zeta+f) + V\cdot\nabla(\zeta+f) = -f\nabla\cdot V \tag{2}$$

By equation of continuity,

$$\nabla\cdot V = -\frac{\partial\omega}{\partial p}$$

Eq. (2) becomes

$$\frac{\partial}{\partial t}(\zeta+f) = -V\cdot\nabla(\zeta+f) + f\frac{\partial\omega}{\partial p} \tag{3}$$

where

$$\omega = \frac{dp}{dt} \doteq -\rho g w$$

Assume now that ω has a vertical parabolic distribution plus the terrain-induced vertical motion.

$$\omega_{(x,y,p,t)} = -\rho_0 g k_1 \frac{p}{p_0} V_0 \cdot \nabla H + \omega_{m(x,y,t)} \left[1 - \left(\frac{p - p_5}{p_0 - p_5}\right)^2\right] \qquad (4)$$

Here p_0, ρ_0, V_0 are the surface pressure, density and wind velocity; H is the height of the terrain; p_5 is an upper-pressure level (to be taken as 500 mb) where vertical motion is strongest; and k_1 is a constant of proportionality.

The term on the right side of Eq. (4) involving $V_0 \cdot \nabla H$ represents the terrain induced vertical motion. Here the surface vertical velocity w_0 is assumed to be proportional to the horizontal wind and the gradient of terrain height H at the surface; i.e. $w_0 = k_1 V_0 \cdot \nabla H$. Moreover, since $\omega_0 = -\rho_0 g w_0$, it follows that

$$\omega_0 = -\rho_0 g k_1 V_0 \cdot \nabla H$$

Finally, the terrain-generated vertical velocity is assumed to decrease linearly with pressure, and thus we arrive at the first term constituting ω in Eq. (4).

The second term of Eq. (4) represents the commonly used parabolic distribution of vertical velocity assumed to be typical of large-scale pressure systems [4]. Where terrain effects are negligible, this term corresponds to low-level "isobaric" velocity divergence and high level convergence (or vice versa), together with the level of non-divergence at p_5 .

Differentiating Eq. (4) with respect to p, substituting it into Eq. (3) and evaluating the result at p_0 gives

$$\frac{\partial \zeta_0}{\partial t} + V_0 \cdot \nabla(\zeta_0 + f) = -\frac{f k_1 \rho_0 g}{p_0} V_0 \cdot \nabla H - \frac{2 f \omega_m}{p_5} \qquad (5)$$

The next step consists of utilizing the first law of thermodynamics to provide a second equation involving ω_m. The non-adiabatic heat addition to the surface-500 mb layer will be assumed to be proportional to the rate at which the surface air parcels are exposed to a changing temperature of the underlying surface.

Expanding the individual change of the potential temperature, θ, and dividing through by θ,

$$\frac{1}{\theta}\frac{d\theta}{dt} = \frac{1}{\theta}\frac{\partial\theta}{\partial t} + \frac{1}{\theta}\mathbf{V}\cdot\nabla_p\theta + \frac{1}{\theta}\omega\frac{\partial\theta}{\partial p} \tag{6}$$

The subscript p at the ∇ operator will be omitted henceforth.

It can be shown from Poisson's equation

$$\theta = T\left(\frac{1000}{p}\right)^{R/c_p}$$

that with pressure held constant

$$\frac{1}{\theta}\frac{\partial\theta}{\partial t} = \frac{1}{\alpha}\frac{\partial\alpha}{\partial t}, \quad \text{and} \quad \frac{1}{\theta}\nabla\theta = \frac{1}{\alpha}\nabla\alpha,$$

where α is the specific volume and R, the universal gas constant. Substituting these identities into Eq. (6) yields

$$\frac{1}{\theta}\frac{d\theta}{dt} = \frac{1}{\alpha}\frac{\partial\alpha}{\partial t} + \frac{1}{\alpha}\mathbf{V}\cdot\nabla\alpha + \frac{1}{\theta}\omega\frac{\partial\theta}{\partial p} \tag{7}$$

From the hydrostatic equation,

$$\alpha = -g\frac{\partial z}{\partial p},$$

substitute into Eq. (7) after multiplying through by α, giving

$$\frac{\alpha}{\theta}\frac{d\theta}{dt} = -g\frac{\partial}{\partial t}\left(\frac{\partial z}{\partial p}\right) - g\mathbf{V}\cdot\nabla\left(\frac{\partial z}{\partial p}\right) + \frac{\alpha}{\theta}\omega\frac{\partial\theta}{\partial p}$$

It follows that

$$\frac{\partial}{\partial t}\left(\frac{\partial z}{\partial p}\right) = -V\cdot\nabla\left(\frac{\partial z}{\partial p}\right) - \sigma\omega - \frac{\alpha}{g\theta}\frac{d\theta}{dt}, \quad \sigma = -\frac{\alpha}{g\theta}\frac{\partial\theta}{\partial p}, \tag{8}$$

Equation (8) states that the local change of the rate of change of the pressure height with respect to pressure is the result of: a) advection, b) vertical motion, and c) the non-adiabatic heating process represented by the last term.

At this stage, the non-adiabatic addition of heat will be assumed proportional to the expression $V_0 \cdot \nabla T_s$ where V_0 is the wind at the surface and T_s is the surface temperature of underlying ocean surface. Hence Eq. (8) may then be expressed in the form

$$\frac{\partial}{\partial t}\left(\frac{\partial z}{\partial p}\right) + V\cdot\nabla\left(\frac{\partial z}{\partial p}\right) + \sigma\omega = k_3 V_0\cdot\nabla T_s \tag{9}$$

where k_3 is the constant of proportionality. Strictly speaking, k_3 is not a constant but may possibly vary with synoptic situations and also vary slowly with time. However, k_3 will be assumed constant for the present investigation.

Now substitute Eq. (4) into Eq. (9) and make geostrophic approximation in the advection term.

$$\frac{\partial}{\partial t}\left(\frac{\partial z}{\partial p}\right) = -V_0\cdot\nabla\left(\frac{\partial z}{\partial p}\right) - \sigma\left\{-g\rho_0 k_1 \frac{p}{p_0} V_0\cdot\nabla H + \omega_m\left[1-\left(\frac{p-p_m}{p_0-p_s}\right)^2\right]\right\}$$
$$+ k_3 V_0\cdot\nabla T_s .$$

By integrating between p_0 and p_s, assuming σ to be a constant, we obtain

$$\frac{\partial h}{\partial t} = -V_0 \cdot \nabla h + \frac{2}{3}\sigma r_5 \omega_m - \frac{3}{4}\sigma g \rho_0 r_5^2 k_1 V_0 \cdot \nabla H + \int_{p_0}^{p_5} (k_3 V \cdot \nabla T_5)\, dp.$$

Here h is the thickness between p_0 and p_5.

In the last term of the preceding equation, V_0 and T_s are independent of pressure, hence

$$\frac{\partial h}{\partial t} = -V_0 \cdot \nabla h + \frac{2}{3}\sigma r_5 \omega_m - \frac{3}{4}\sigma g \rho_0 r_5^2 k_1 V_0 \cdot \nabla H + k_2 V_0 \cdot \nabla T_5 \qquad (10)$$

where k_2 is a new constant.

Solving Eq. (10) for ω_m,

$$\omega_m = \frac{3}{2\sigma r_5}\left(\frac{\partial h}{\partial t} + V_0 \cdot \nabla h + \frac{3}{4}\sigma g \rho_0 r_5^2 k_1 V_0 \cdot \nabla H - k_2 V_0 \cdot \nabla T_5\right)$$

and substituting it into Eq. (5) gives

$$\frac{\partial f_0}{\partial t} + V_0 \cdot \nabla(f_0 + f) = -\frac{f k_1 g \rho_0}{p_0} V_0 \cdot \nabla H - \frac{2f}{r_5}\left[\frac{3}{2\sigma r_5}\left(\frac{\partial h}{\partial t} + V_0 \cdot \nabla h + \frac{3}{4}\sigma g \rho_0 r_5^2 k_1 V_0 \cdot \nabla H - k_2 V_0 \cdot \nabla T_5\right)\right]$$

Rearranging,

$$\frac{\partial f_0}{\partial t} + \frac{3f}{\sigma r_5^2}\frac{\partial h}{\partial t} = -V_0 \cdot \nabla(f_0 + f) - \left(\frac{f k_1 g \rho_0}{p_0} + \frac{9 g \rho_0 k_1 f}{4 r_5}\right) V_0 \cdot \nabla H - \frac{3f}{\sigma r_5^2} V_0 \cdot \nabla h + \frac{3f}{\sigma r_5^2} k_2 V_0 \cdot \nabla T_5,$$

$$\therefore \frac{\partial}{\partial t}\left(f_0 + \frac{3f}{\sigma r_5^2} h\right) = -V_0 \cdot \nabla\left(f_0 + f + \frac{11 \rho_0 g k_1 f}{2 r_0} H + \frac{3f}{\sigma r_5^2} h - \frac{3f k_2}{\sigma r_5^2} T_5\right) \qquad (11)$$

Now, we make the geostrophic approximation for ζ_0 in Eq. (11).

$$\zeta_0 = \frac{4g m^2}{f d^2}(\bar{z}_0 - z_0)$$

$$\frac{\partial}{\partial t}\left[\frac{4g m^2}{f d^2}(\bar{z}_0 - z_0) + \frac{3f}{\sigma \rho_s^2} h\right]$$

$$= -V_0 \cdot \nabla\left[\frac{4g m^2}{f d^2}(\bar{z}_0 - z_0) + f + \frac{11 \rho_0 g k_1 f}{8 \rho_0^2} H + \frac{3f}{\sigma \rho_s^2} h - \frac{3 f k_2}{\sigma \rho_s^2} T_s\right]$$

According to Fjortoft, the horizontal variation of $\frac{m^2}{f}$ may be neglected in comparison to $(\bar{z}_0 - z_0)$. With multiplication by $\frac{f d^2}{4g m^2}$, we obtain

$$\frac{\partial}{\partial t}\left[\bar{z}_0 - z_0 + \frac{3 f^2 d^2}{4 g m^2 \sigma \rho_s^2} h\right]$$

$$= -V_0 \cdot \nabla\left[\bar{z}_0 - z_0 + \int_0^{\varphi} \frac{f d^2}{4 g m^2} \frac{\partial f}{\partial \varphi} \delta\varphi + \frac{11 f^2 d^2 \rho_0 k_1}{8 m^2 \rho_0} H + \frac{3 f^2 d^2}{4 g m^2 \rho_s^2 \sigma} h - \frac{3 k_2 f^2 d^2}{4 g m^2 \sigma \rho_s^2} T_s\right] \quad (12)$$

The coriolis force term on the right side of Eq. (12) has been manipulated as follows:

$$\frac{\partial f}{\partial \varphi} = \frac{\partial}{\partial \varphi}(2\Omega \sin\varphi) = 2\Omega \cos\varphi$$

$$\int_0^{\varphi} \frac{f d^2}{4 g m^2} \frac{\partial f}{\partial \varphi} \delta\varphi = \int_0^{\varphi} \frac{d^2 2\Omega \sin\varphi \, 2\Omega \cos\varphi}{4 g m^2} \delta\varphi$$

$$= \frac{d^2 \Omega^2}{g} \int_0^{\varphi} \frac{\sin\varphi \cos\varphi}{m^2} \delta\varphi = G$$

Now let

$$C = \frac{3 f^2 d^2}{4 g m^2 \rho_s^2 \sigma}$$

$$F = \frac{11 f^2 d^2 \rho_0 g k_1}{8 g m^2 \rho_0^2} H$$

$$N = -\frac{3 k_2 f^2 d^2}{4 g m^2 \sigma \rho_s^2}$$

Therefore Eq. (12) becomes

$$\frac{\partial}{\partial t}\left[\bar{Z}_0 - Z_0 + Ch + G + F + NT_s\right]$$

$$= -V_0 \cdot \nabla\left[\bar{Z}_0 - Z_0 + Ch + G + F + NT_s\right] \qquad (13)$$

The function NT_s varies very slowly with time and may be assumed to be a constant for the normal forecast period. The functions G and F depend on geographical position only and are invariant with time, hence they may be inserted on the left side of Eq. (13). Equation (13) shows that the quantity $(\bar{Z}_0 - Z_0 + Ch + G + F + NT_s)$ is conservative with respect to wind field at P_0. By using the geostrophic approximation for V_0, i.e.

$$u_0 = -\frac{g}{f}\frac{\partial Z_0}{\partial y} \quad ; \quad v_0 = \frac{g}{f}\frac{\partial Z_0}{\partial x}$$

Eq. (13) may be written in Jacobian form as

$$\frac{\partial}{\partial t}\left[\bar{Z}_0 - Z_0 + Ch + G + F + NT_s\right]$$

$$= -\frac{g}{f} J\left[Z_0, \bar{Z}_0 - Z_0 + Ch + G + F + NT_s\right] \qquad (14)$$

In order to arrive at a more conservative field for advecting the conservative property, the Jacobian identity, J(x,y) = J(x+y,y), may be applied to Eq. (14), giving

$$\frac{\partial}{\partial t}\left[\bar{Z}_0 - Z_0 + Ch + G + F + NT_s\right]$$

$$= -\frac{g}{f} J\left[\bar{Z}_0 + Ch + G + F + NT_s, \bar{Z}_0 - Z_0 + Ch + G + F + NT_s\right] \qquad (15)$$

The use of this form implies that the $[\bar{Z}_0 + Ch + G + F + NT_s]$ field is expected to be more conservative than the Z_0 field for advection purposes. This is not necessarily always the case since the thickness field appears in the advecting quantity. Nevertheless, in the examples tested, Eq. (15) gave good results.

To depict the local change of $[\bar{Z}_0 - Z_0 + Ch + G + F + NT_s]$ we shall advect this function for a short time interval, say twelve hours or twenty-four hours. Denote this change by Δ . Since G, F and NT_s are not functions of time,

$$\Delta[\bar{Z}_0 - Z_0 + Ch + G + F + NT_s]$$

$$= \Delta[\bar{Z}_0 - Z_0 + Ch] = -A \tag{16}$$

Moreover, $h = Z_s - Z_0$

$$\Delta[\bar{Z}_0 - Z_0 + Ch] = \Delta[\bar{Z}_0 - Z_0 + C(Z_s - Z_0)]$$

$$= \Delta[\bar{Z}_0 - (1+C)Z_0 + CZ_s] = -A$$

$$\therefore \Delta Z_0 = \frac{1}{1+C}[A + \Delta\bar{Z}_0 + C\Delta Z_s] = B + \frac{1}{1+C}\Delta\bar{Z}_0 \tag{17}$$

where $B = \frac{1}{1+C}(A + C\Delta Z_s)$

Taking the space average over Eq. (17) and substituting back to Eq. (17), yields

$$\Delta Z_0 = B + \frac{1}{1+C}\left[\bar{B} + \frac{1}{1+C}\Delta\bar{\bar{Z}}_0\right]$$

$$= B + \frac{1}{1+C}\bar{B} + \frac{1}{(1+C)^2}\Delta\bar{\bar{Z}}_0 .$$

Averaging n times,

$$\Delta Z_0 = B + \frac{1}{1+C}\bar{B} + \frac{1}{(1+C)^2}\bar{\bar{B}} \cdots\cdots + \frac{1}{(1+C)^{n+1}}\Delta\overbrace{\bar{Z}_0}^{n+1} \tag{18}$$

However, this series converges rapidly; and, as shown by Fjortoft [2], it can be approximated as

$$\Delta Z_0 \doteq B + \frac{2}{1+C}\bar{B} \tag{19}$$

In the cases tested in this investigation, it was found that the second term on the right side of Eq. (19) can be neglected except when a marked change is indicated. In the routine work where a time saving is of great importance, $\Delta Z_0 \doteq B$ can be used without much sacrifice in accuracy. In utilizing the high speed electronic computer, Eq. (16) could be solved to any desired accuracy.

3. Procedure

In order to provide a comparison to Reed's results [5], the same case has been chosen for prognostication. Two other series were also chosen for testing purposes. One series has the storm located in the Gulf of Alaska. Each series contains three consecutive periods with a time interval of twelve hours. Except in the same case as Reed's, where the prognosis without heating effect was already available, two prognoses for each case have been obtained, one omitting and the other including the heating effect.

By omitting the heating effect, Eq. (15) becomes

$$\frac{\partial}{\partial t}\left[\bar{Z}_o - Z_o + Ch + G + F\right] = -\frac{g}{f}J\left[\bar{Z}_o + Ch + G + F,\ \bar{Z}_o - Z_o + Ch + G + F\right] \qquad (20)$$

The following steps are carried out in each prognostication:

(1). A space-mean chart for Z_o is graphically constructed using a grid distance of 600 km.

(2). With C = 0.5, the current thickness chart is multiplied by 1/2 (this is achieved by simply tracing every other line on the thickness chart) and added to $\bar{Z}_o$.

(3). Next the result of step (2) is added to the (G + F) function provided by Haltiner and Hesse [3].

(4). With $N = -0.1\ \frac{100\ ft}{^{\circ}F}$ over the ocean and N = -0.05 over the land area of Alaska (see Section 4), a (NT_s) function chart was constructed based on the monthly mean ocean surface isotherms published by the Hydrographic Office and the current reported temperatures over the land. (Fig. 19). This chart of $f(NT_s)$ was added to the result of (3). Note this step is unnecessary if non-adiabatic heating is omitted. Also it is

suggested, since monthly mean surface temperature isotherms over the ocean are used, a chart of ($G + F + NT_s$ ocean) function may be prepared for each winter month. This will combine step (4) into step (3) if the (NT_s) function over land is also approximated by the monthly mean isotherms over the land. Up to this step, a chart of function of ($\bar{Z}_o + Ch + G + F + NT_s$) has been obtained and will be referred to as steering chart henceforth.

(5). The Z_o chart is subtracted from steering chart to obtain the quantity to be advected.

(6). Next advect the quantity obtained in step (5) with the steering chart for twelve-hour intervals.

(7). Subtract the result of step (6) from the result of step (5) to get A.

(8). Add $1/2 \Delta Z_c$ to A and multiply the result by 2/3 to obtain B.

(9). Average B to get $\bar{B}$ and multiply by 4/3.

(10). Add the result of (9) to (8), to get ΔZ_o.

(11). Add ΔZ_o to the initial 1000-mb chart to give the prognostic 1000-mb chart of twelve hours later.

4. Discussion

In this investigation, three constants are of major importance, namely; C, k_1, and N. Of these three constants, k_1 has been discussed in the Haltiner and Hesse paper [3], and only C and N will be discussed here.

(1). The constant C.

Several values of C have been used by various investigators. In the present investigation, the value of C = 0.5 fits best in the cases tested. Values lower than this will give an advection field too weak, while higher values give an advecting field too strong.

(2). The constant N.

In this investigation the primary interest is in the area of outflow of cP air from inland Alaska to the sea. Over the ocean the value of constant N was found empirically to be $-0.1 \frac{1000\,T}{°F}$. In the non-adiabatic modification of an air mass, the processes which actually take place are not simple. The degree and rate of the modification are dependent upon many factors such as: a) the temperature difference between the cP air mass and sea surface; b) the roughness of the sea surface; c) the wind speed over the sea surface; d) the length of time the air mass has been over the ocean; e) the stability of the air mass; f) the moisture content of the air mass; etc. The inter-relations among these factors are not well known quantitatively; consequently, it is difficult to determine in a specific case the relative importance of the various factors. For example, air moving with a higher speed is not necessarily being modified proportionately more than air moving at a much lower speed. The reason for this is that the modification is not only a function of the distance over which the air has traveled from the coast, but also a function of the time the air mass has been over the ocean. The expression $k_2 V_0 \cdot \nabla T_s$ implies that when the value of V_0 is doubled, the amount of modification will

double, which is not necessarily true. Thus, the determination of the value of N is a matter of compromise of the many different influences. For the relatively small sample tested, the value of N = -0.1 appears to be the best choice thus far. However, application of this value shows considerable improvement over the other models which treat the non-adiabatic heating effect in a different way.

In the course of this investigation, it appeared that the advecting field tends to move the high pressure cell down stream over inland Alaska, with the result that the prognostic pressure height was too high over the southwestern side of the High and too low over the southeastern side of the High. For example, in the case 1500 GMT January 4, 1956 to 0300 GMT January 5, the high was built up on the east side. In this situation, an attempt was made to apply the non-adiabatic effect over inland Alaska by putting N = -0.05, obtaining a $f(NT_s)$ based on the isotherms on the current surface map. Considerable improvement resulted. Such an approach provides a continuous temperature field from the inland out to the sea. This value of N was also applicable to the other inland cases. The combined functions (NT_s) for the land and the sea are shown in Figs. 19, 20, 21, 22. From these figures, it seems feasible to use the monthly mean temperature over Alaska land area as the basis of $f(NT_s)$ over land, so that step (4) can be entirely incorporated into step (3) by preparing a single chart of $f(G + F + NT_s)$ for each winter month. Thus a considerable amount of time can be saved in daily routine work. Since the non-adiabatic cooling process over the land, probably mostly due to radiational cooling, is beyond the scope of this investigation, no further discussion will be given.

In addition to the empirical determination of constants, another aspect at the advecting stage in the procedure warrants some discussion. As the air mass moves southward over an increasing temperature field, the

air mass will be warmed up from below. An assumption was made that the air parcel directly in contact with the sea surface will immediately acquire the same temperature as that of the sea surface. In this case, the air mass tends to be unstable. This instability will enhance the upward heat transport, and so increase the modification. On the contrary, when the air mass moves northward over a decreasing temperature field, by the same assumption it tends to be stabilized. In the first case, the thickness of the lower layer will increase and in the latter case the thickness will decrease. However the magnitude in the first case of increasing thickness is normally much larger than the magnitude in the latter case of decreasing thickness. Because of this consideration, an attempt was made to advect less distance in cold advection and to advect the full distance in warm advection. However, this did not improve the results, since the property to be advected is a combination of $\bar{Z}_o$, Z_o, Ch, G, F, and NT_s, and not a function of NT_s alone. As a matter of fact, since the value of N has been determined empirically, it represents a compromise of all the various influences.

5. Results

The results of the tests are displayed in Table I which shows the comparison of the series, with and without non-adiabatic warming or cooling. The statistical parameters computed were based on a seventy-point grid of which forty-seven points were over the sea. These grid points are the intersections of the meridians and latitude parallels which are 5° apart extending from longitude 165°W to longitude 120°W and from latitude 65°N down to latitude 30°N. Due to the convergence of meridians, the points are denser over the northern part of the area. Since the area of denser points is inland and coastal Alaska, which is a more critical area, the values in Table I are more conservative and do not exaggerate the improvement due to the inclusion of the non-adiabatic heating.

TABLE I

Case	Correlation Coefficient of height change (total area of 70 points)		RMS error (non-adiabatic heating omitted)	RMS error (non-adiabatic heating included)	area
	heating omitted	heating included			
1500 GMT January 4, 1956 to 0300 GMT January 5, 1956	0.67*	0.89 (0.74*)	225*	(179*) 91.4	Total (70 points)
			293*	(193*) 85	Ocean (47 points)
0000 GMT January 6, 1959 to 1200 GMT January 6, 1959	0.69	0.78	133	115	Total
			126	109	Ocean
1200 GMT January 6, 1959 to 0000 GMT January 7, 1959	0.52	0.74	141	95	Total
			92	66	Ocean
0000 GMT January 7, 1959 to 1200 GMT January 7, 1959	0.66	0.79	147	67	Total
			105	68	Ocean
Average	0.635	0.80	161.5	92	Total
			154	82	Ocean

* after Reed.
RMS error in units of feet.

Figs. 1 to 16 indicate the results of four cases. These are: Case 1) 1500 GMT January 4, 1956 to 0300 GMT January 5, 1956; Cases 2, 3, 4) 0000 GMT January 13, 1959 to 1200 GMT January 14, 1959, consisting of three consecutive prognoses. The other three cases from 0000 GMT January 13, 1959 to 1200 GMT January 14, 1959 are not shown. It has also been found that the addition of term NT_s gives no improvement when a cyclone comes from the central North Pacific area; however, neither is there a decrease in accuracy when $f(NT_s)$ is included.

It can be seen from the figures that the greatest improvement in the prognostic pressure heights is found over the area on the west of the storm which is the normal location of the cP air. This was true in all the cases tested.

On the basis of the sample tested it may be concluded that this model shows very good promise. However, further testing would be desirable to determine the best values of the various constants. The non-adiabatic heating term can readily be incorporated into the programming of baroclinic models for the electronic computer on which further testing would be greatly facilitated. There is obviously a considerable saving in time compared to the Reed method when this model is applied manually in the graphical technique.

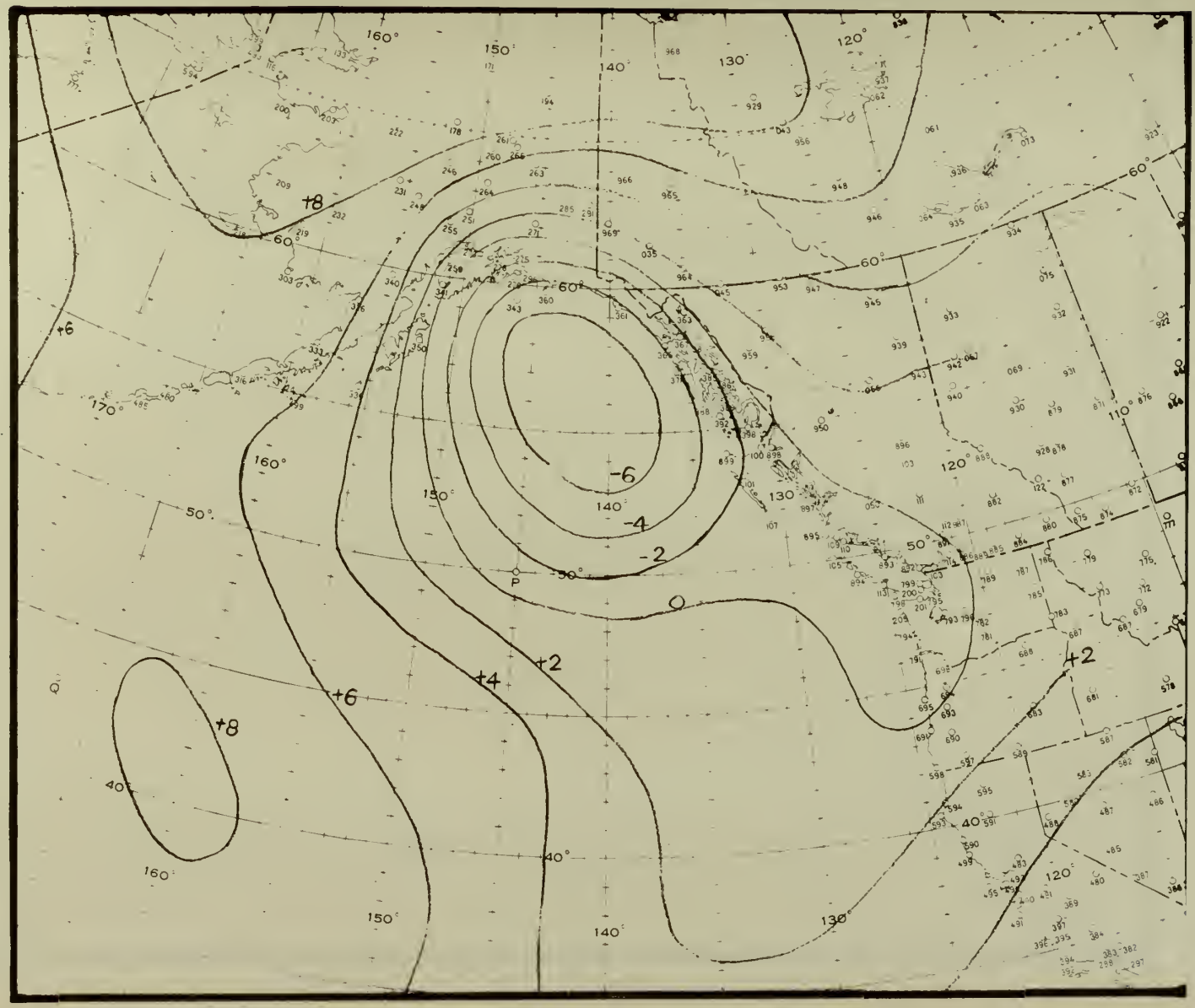

Fig. 1. 1000-mb chart for 1500 GMT 4 January 1956.

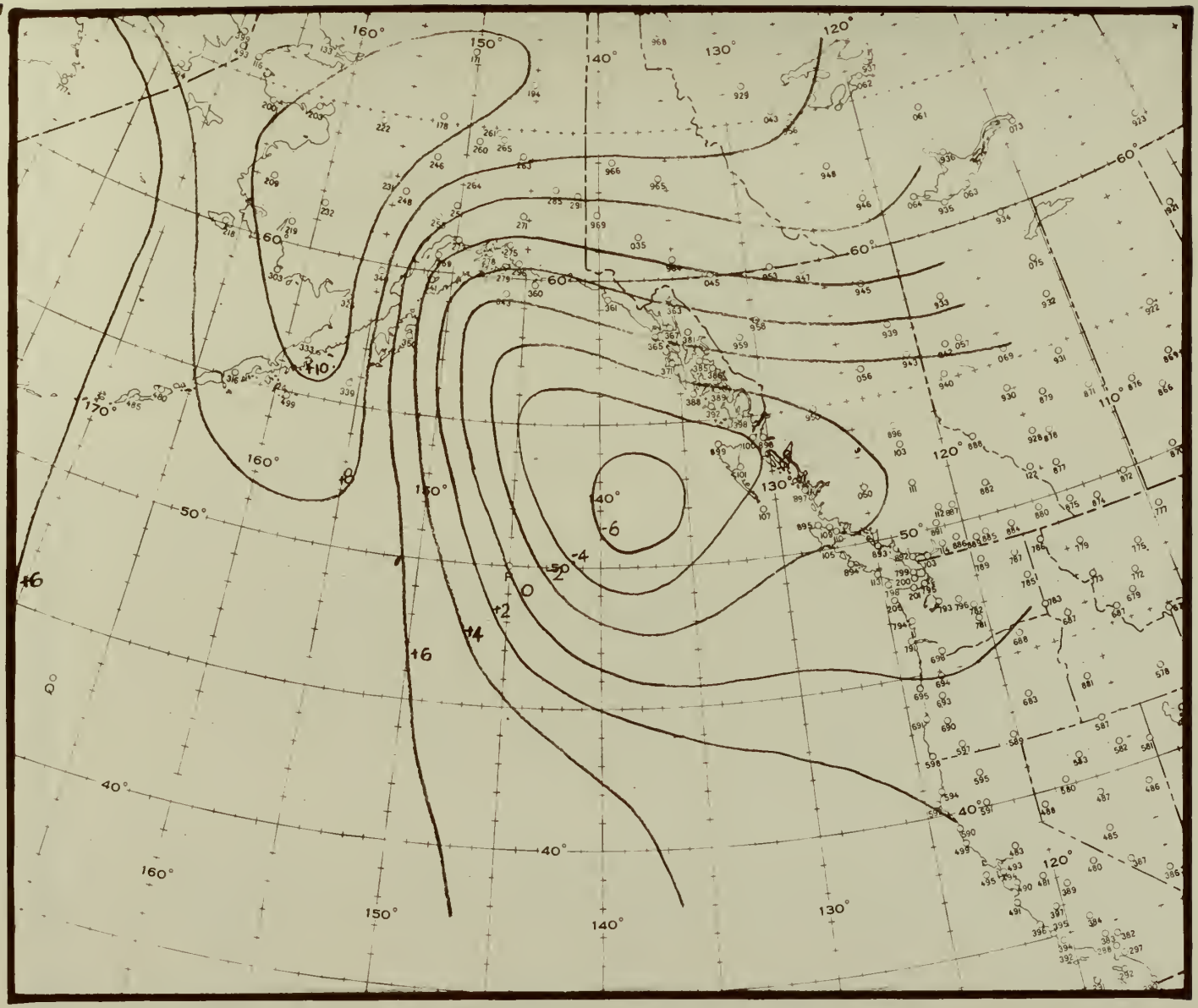

Fig. 2. 1000-mb prognostic chart for 0300 GMT 5 January 1956, without heating effect. After Reed.

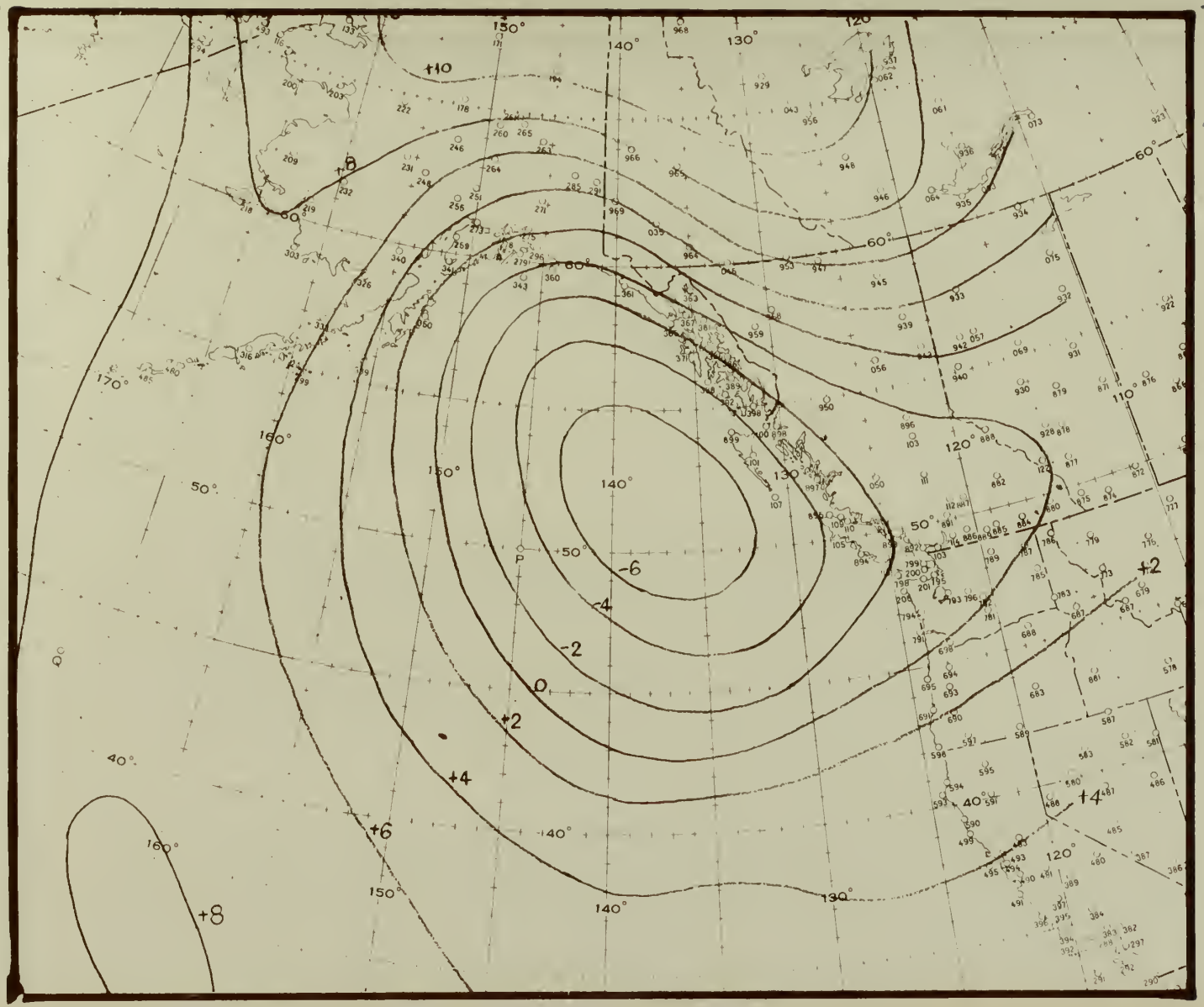

Fig. 3. Actual 1000-mb chart for 0300 GMT 5 January 1956.

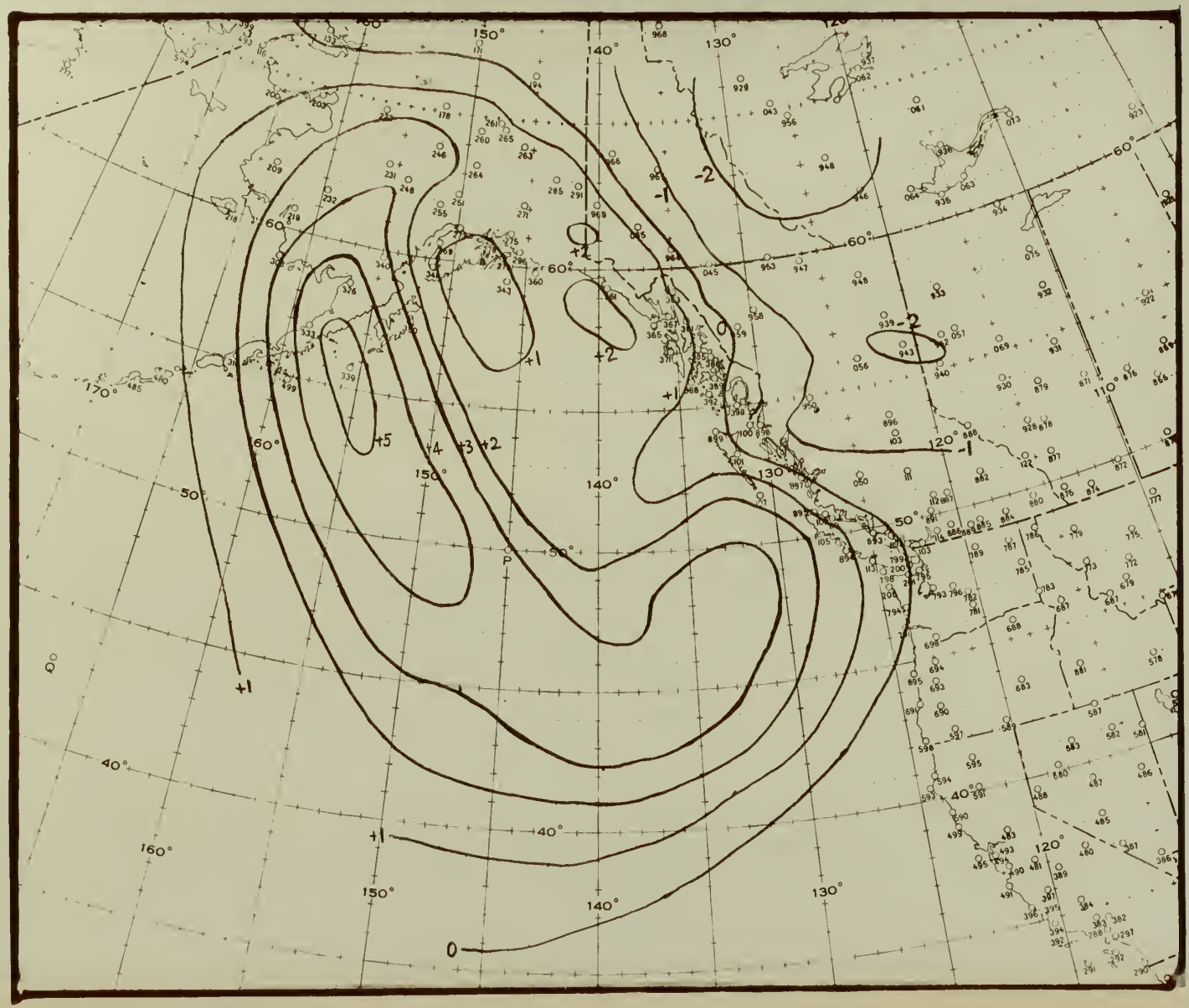

Fig. 4. Prog. minus actual. (Fig. 2 minus Fig. 3).

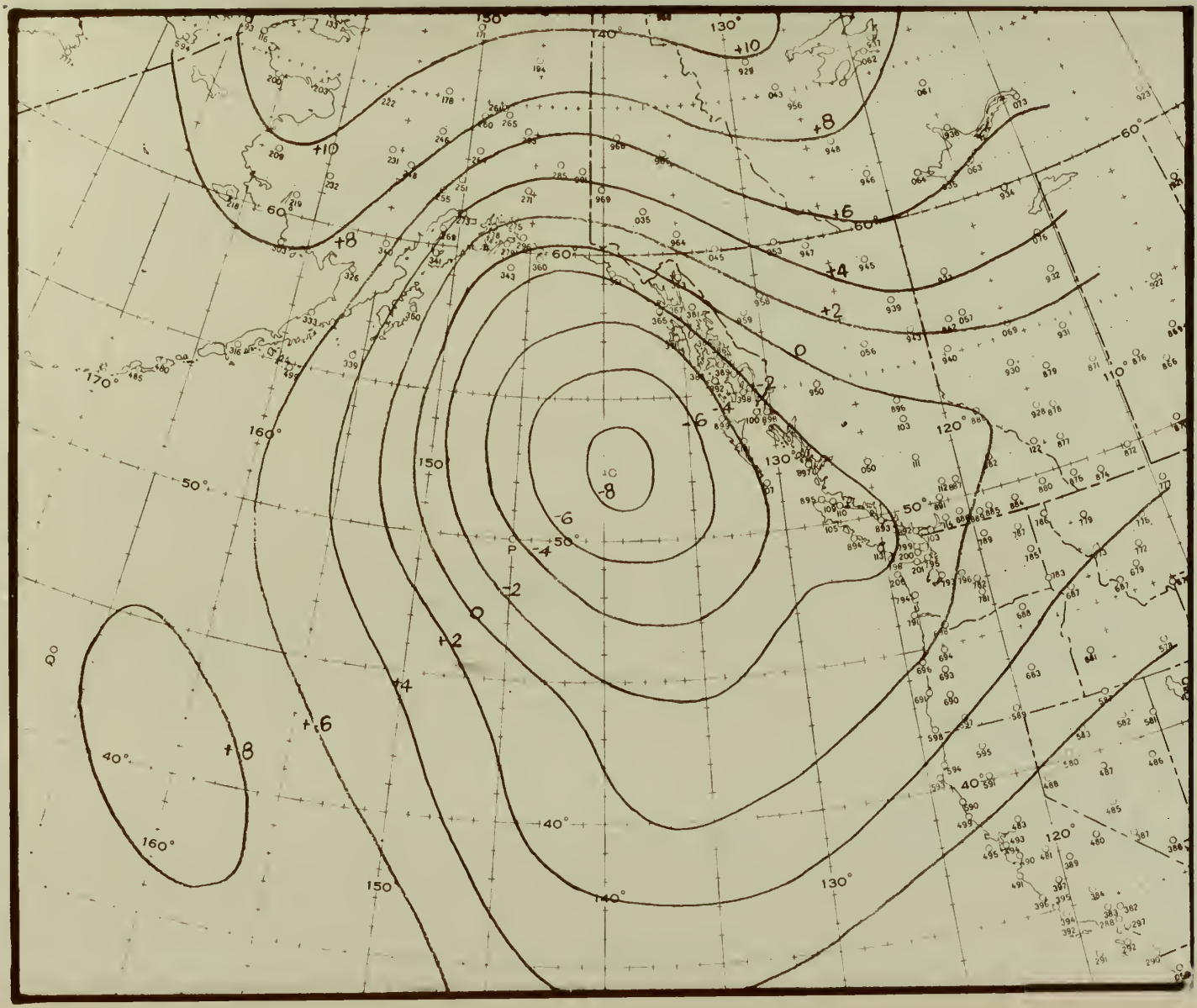

Fig. 5. 1000-mb prognostic chart for 0300 GMT 5 January 1956, with heating effect.

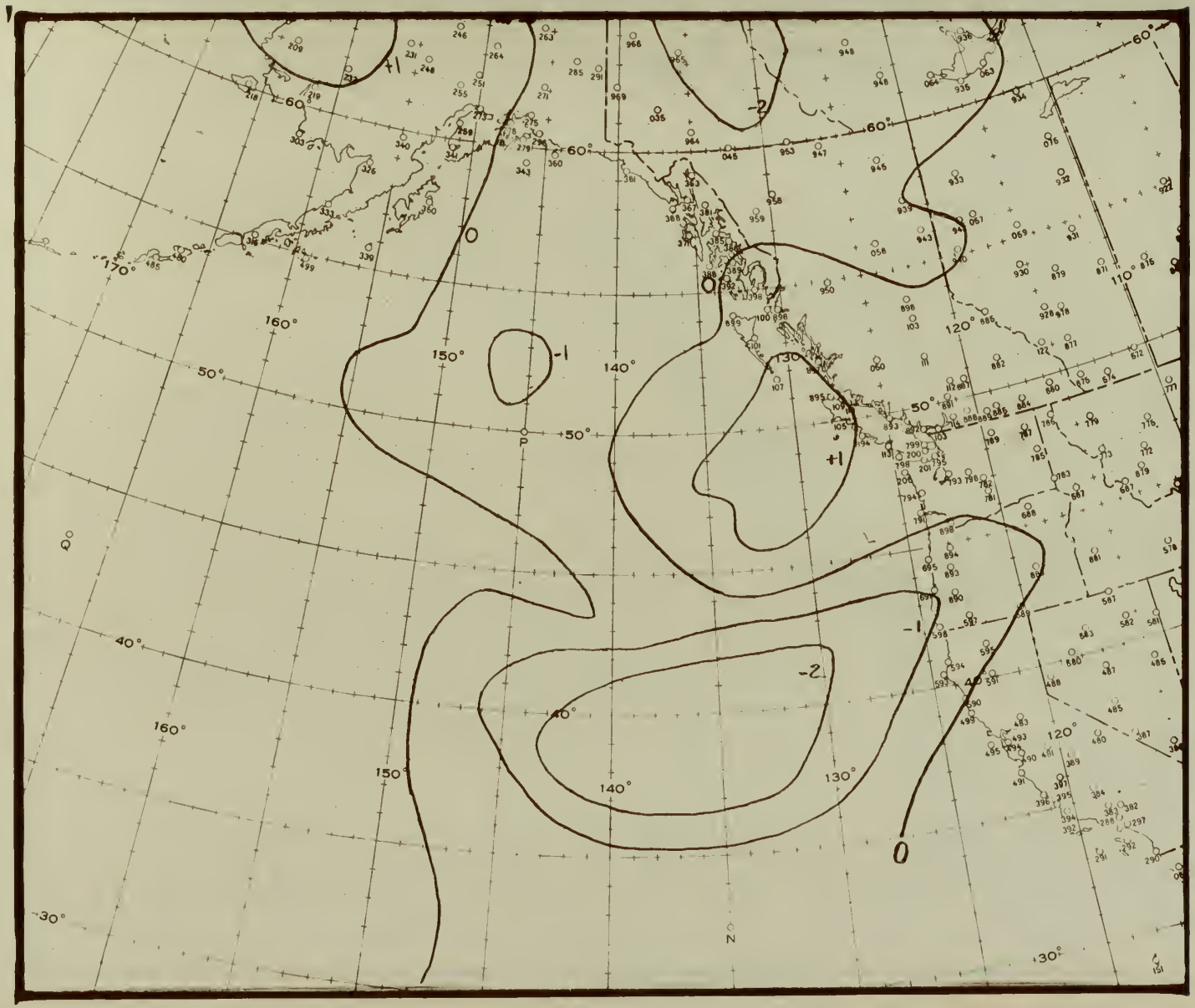

Fig. 6. Prog. with heating effect, minus actual (Fig. 5 minus Fig. 3).

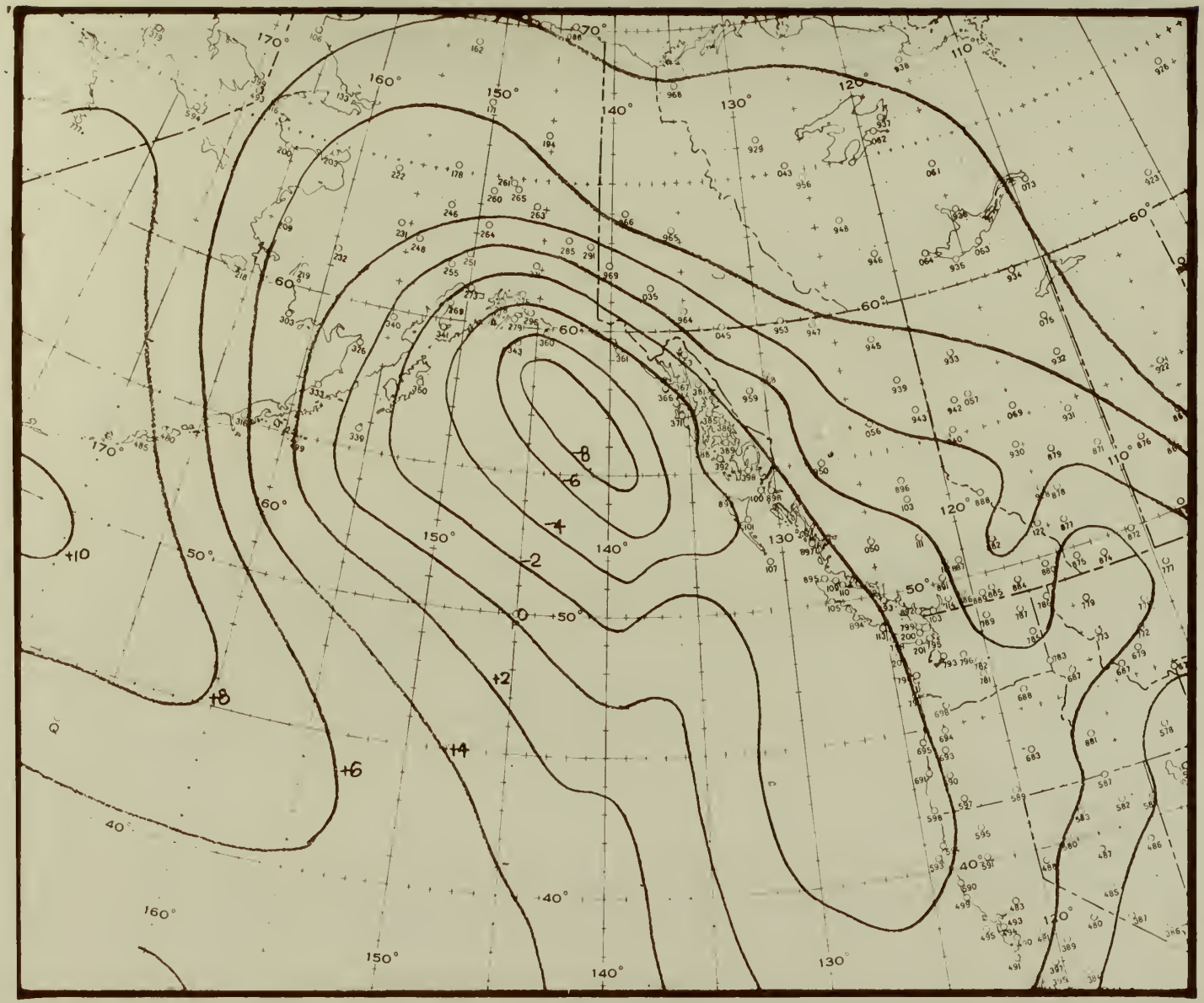

Fig. 7. 1000-mb chart for 0000 GMT 6 January 1959.

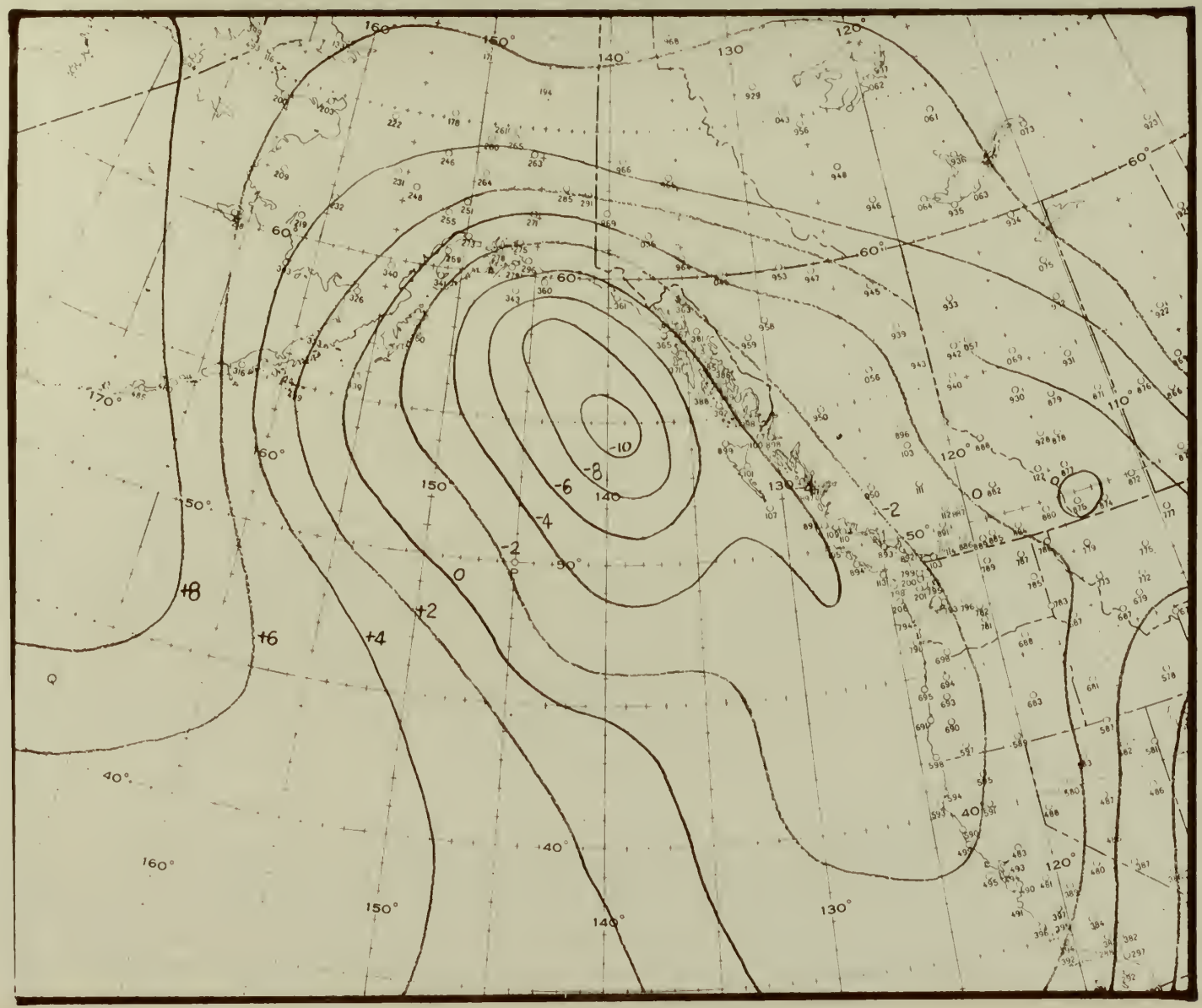

Fig. 8. 1000-mb prognostic chart for 1200 GMT 6 January 1959, without heating effect.

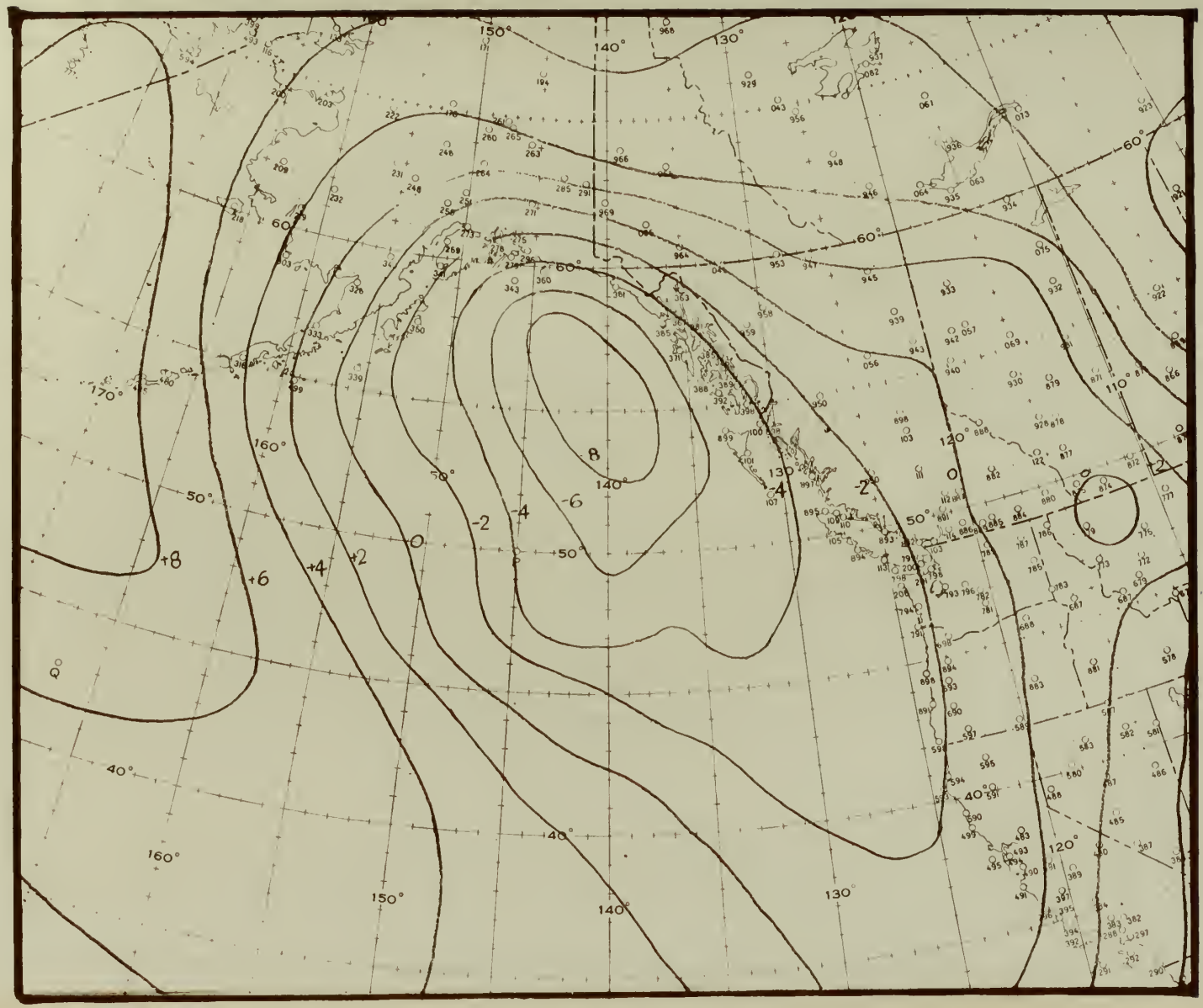

Fig. 9. 1000-mb prognostic chart for 1200 GMT 6 January 1959, with heating effect.

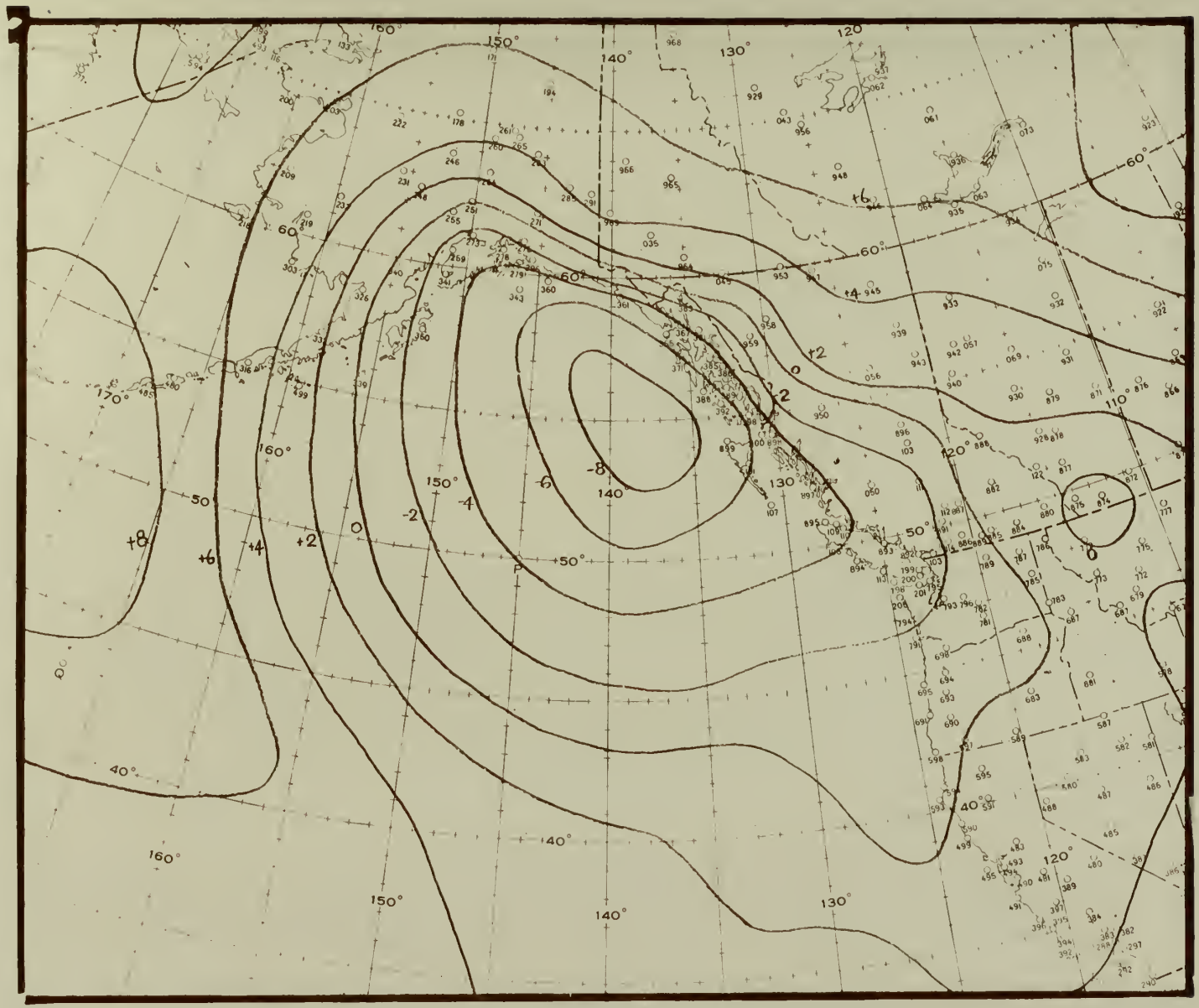

Fig. 10. Actual 1000-mb chart for 1200 GMT 6 January 1959.

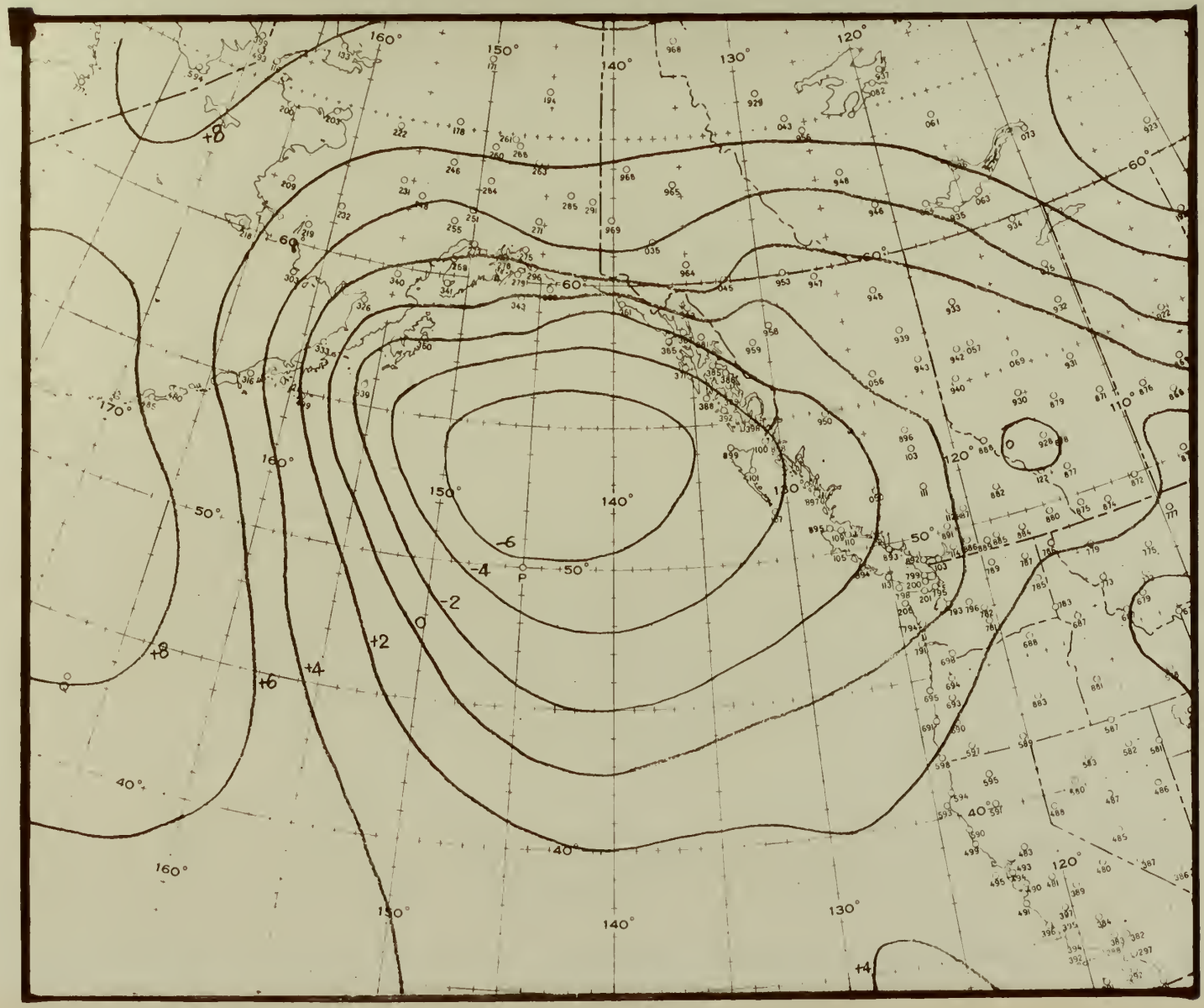

Fig. 11. 1000-mb prognostic chart for 0000 GMT 7 January 1959. without heating effect.

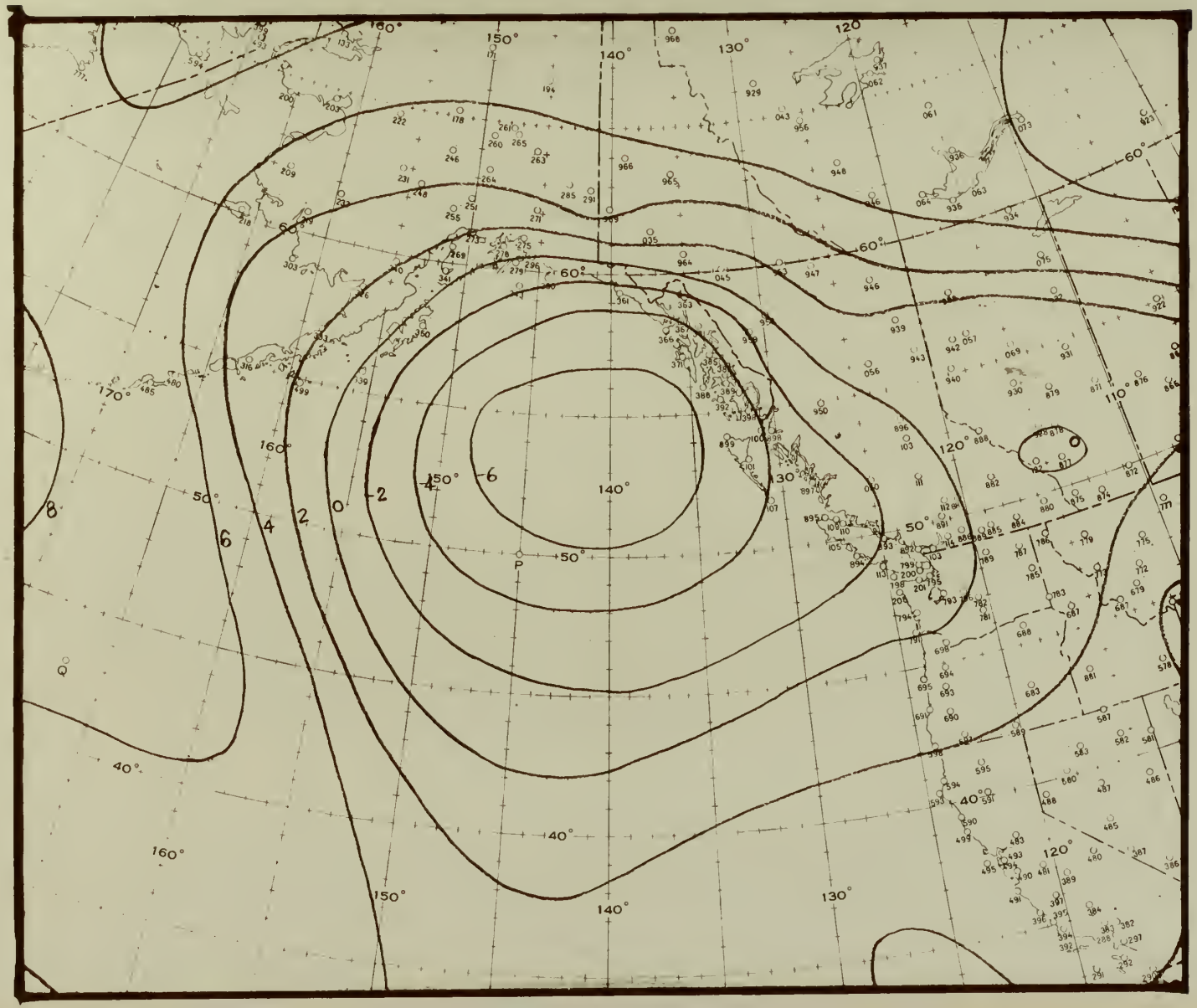

Fig. 12. 1000-mb prognostic chart for 0000 GMT 7 January 1959, with heating effect.

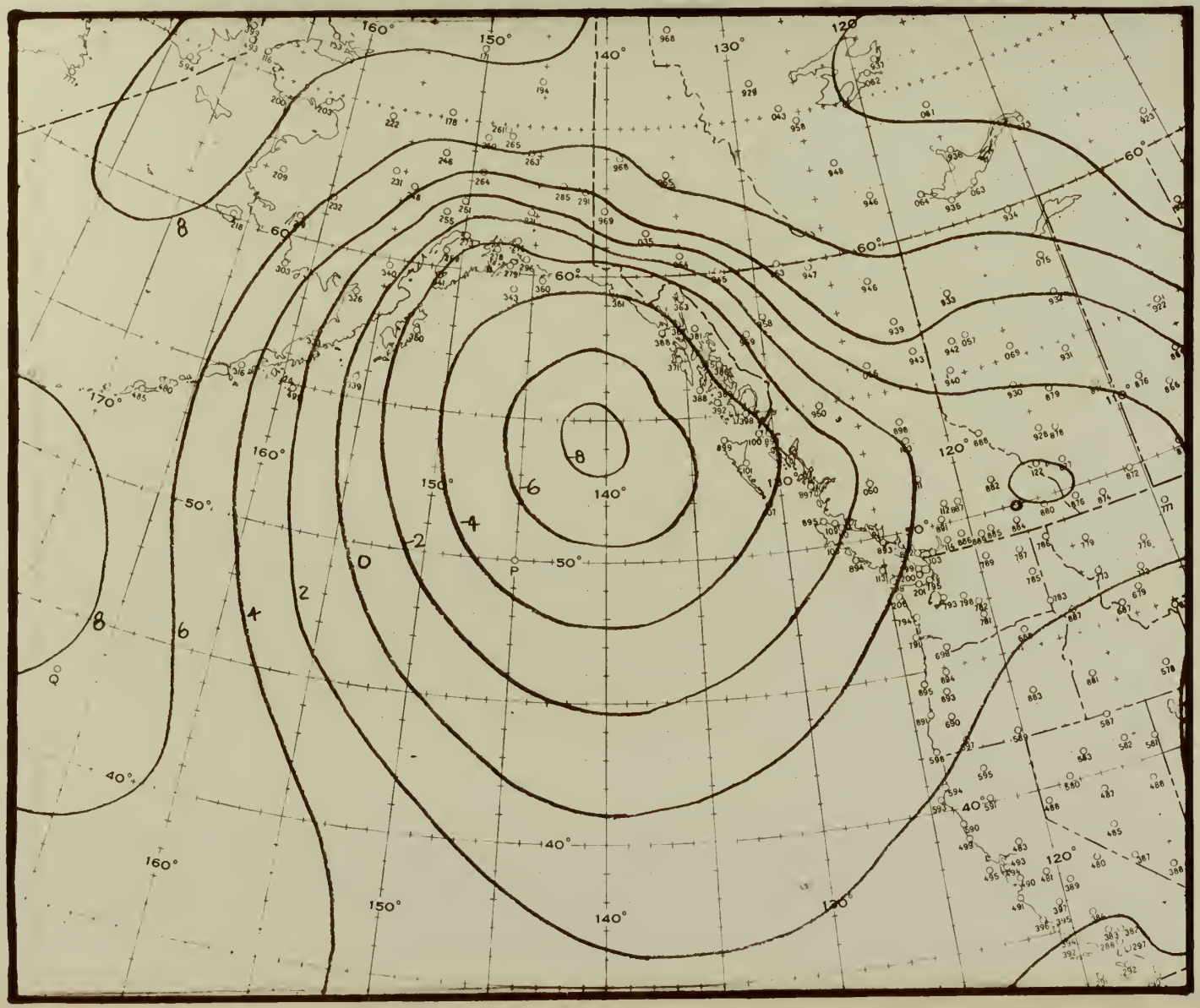

Fig. 13. Actual 1000-mb chart for 0000 GMT 7 January 1959.

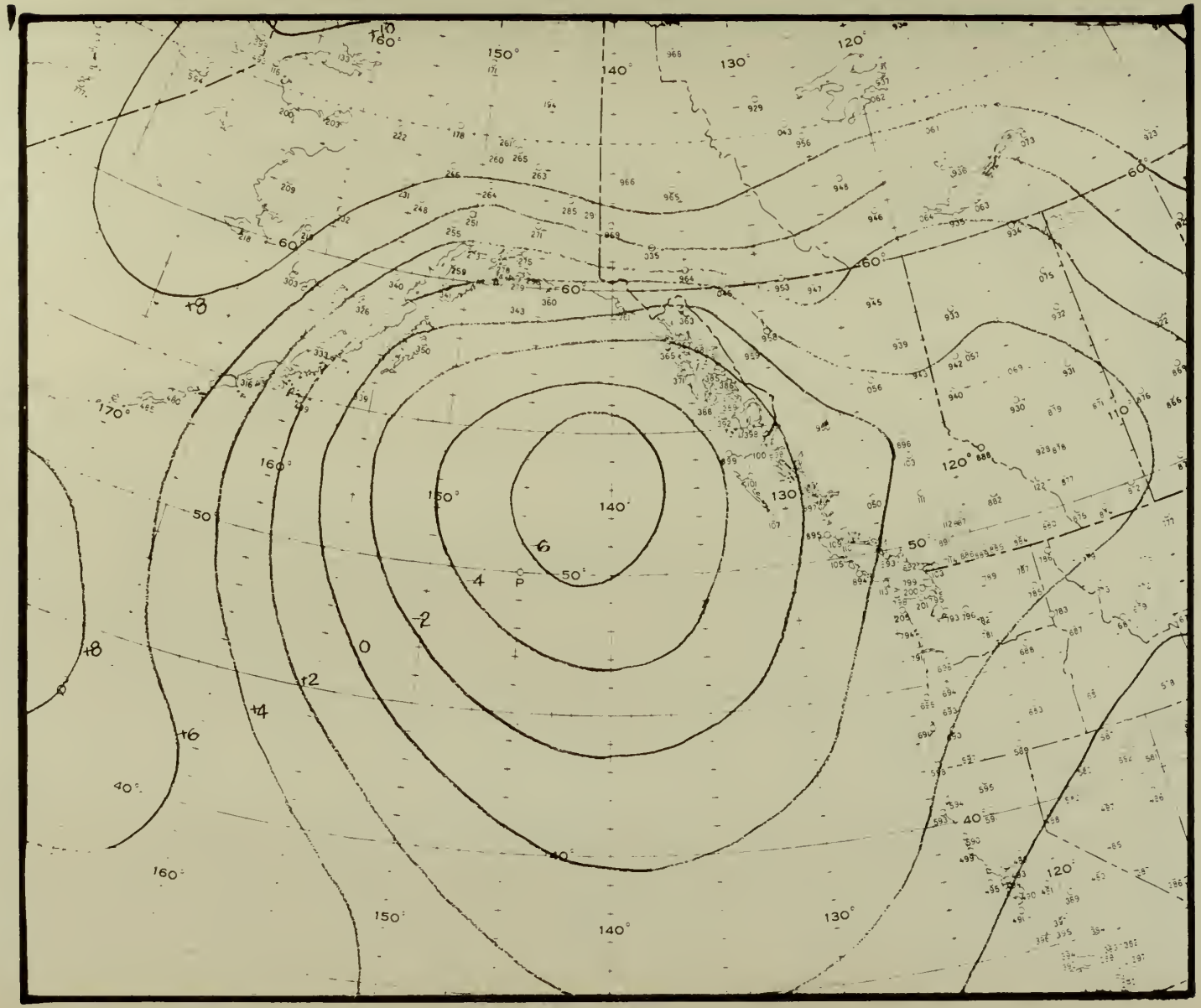

Fig. 14. 1000-mb prognostic chart for 1200 GMT 7 January 1959, without heating effect.

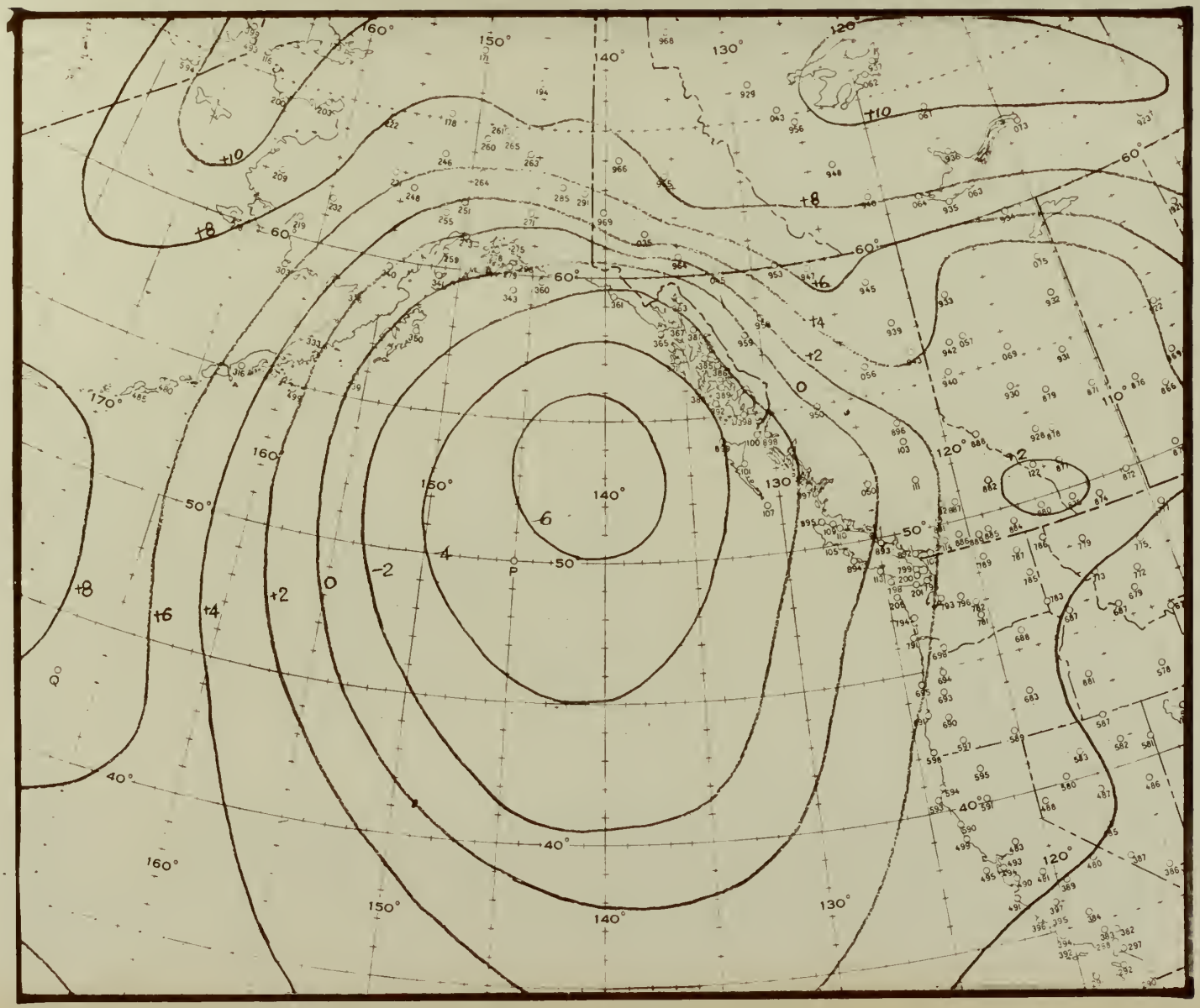

Fig. 15. 1000-mb prognostic chart for 1200 GMT January 1959, with heating effect.

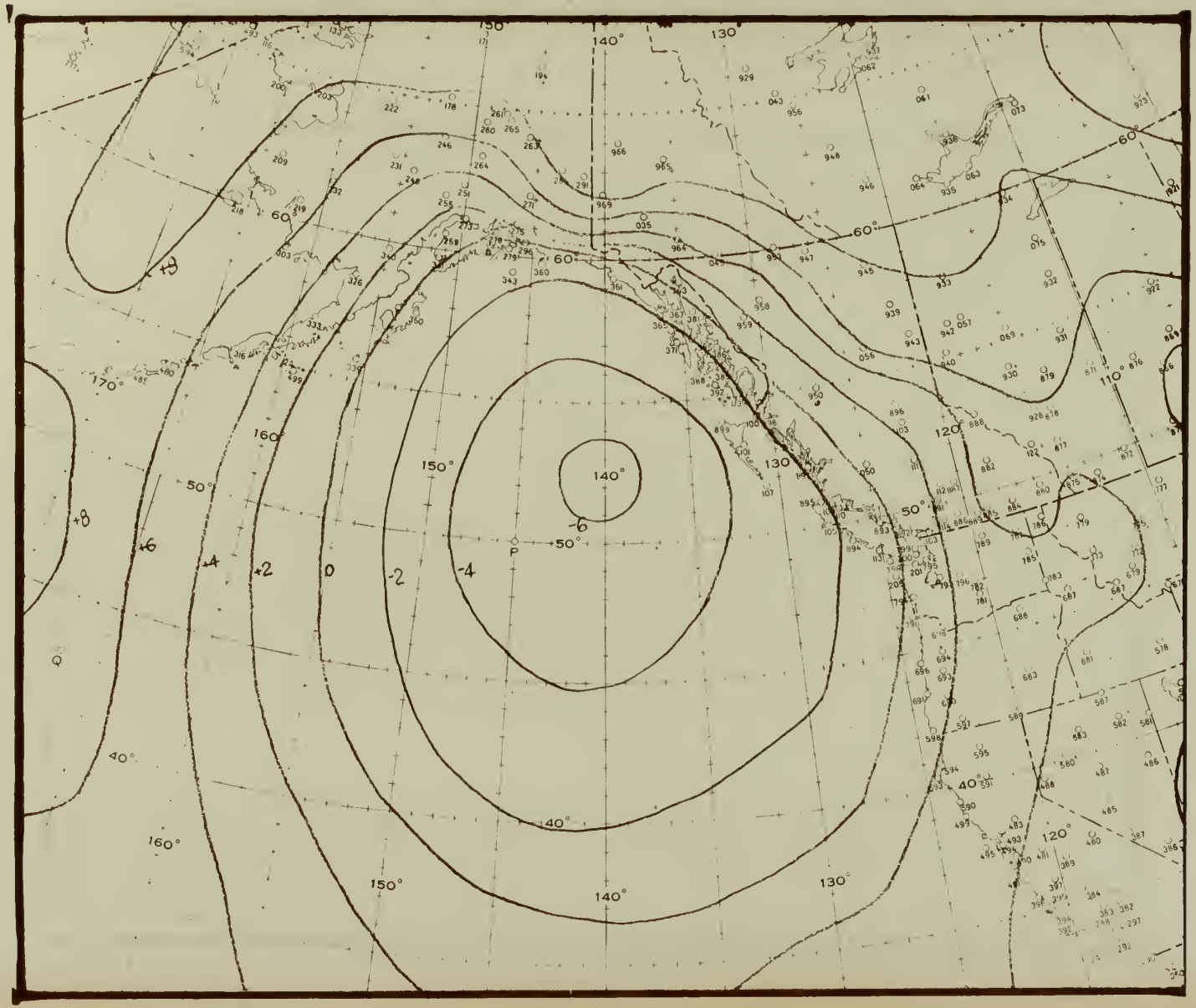

Fig. 16. Actual 1000-mb chart for 1200 GMT 7 January 1959.

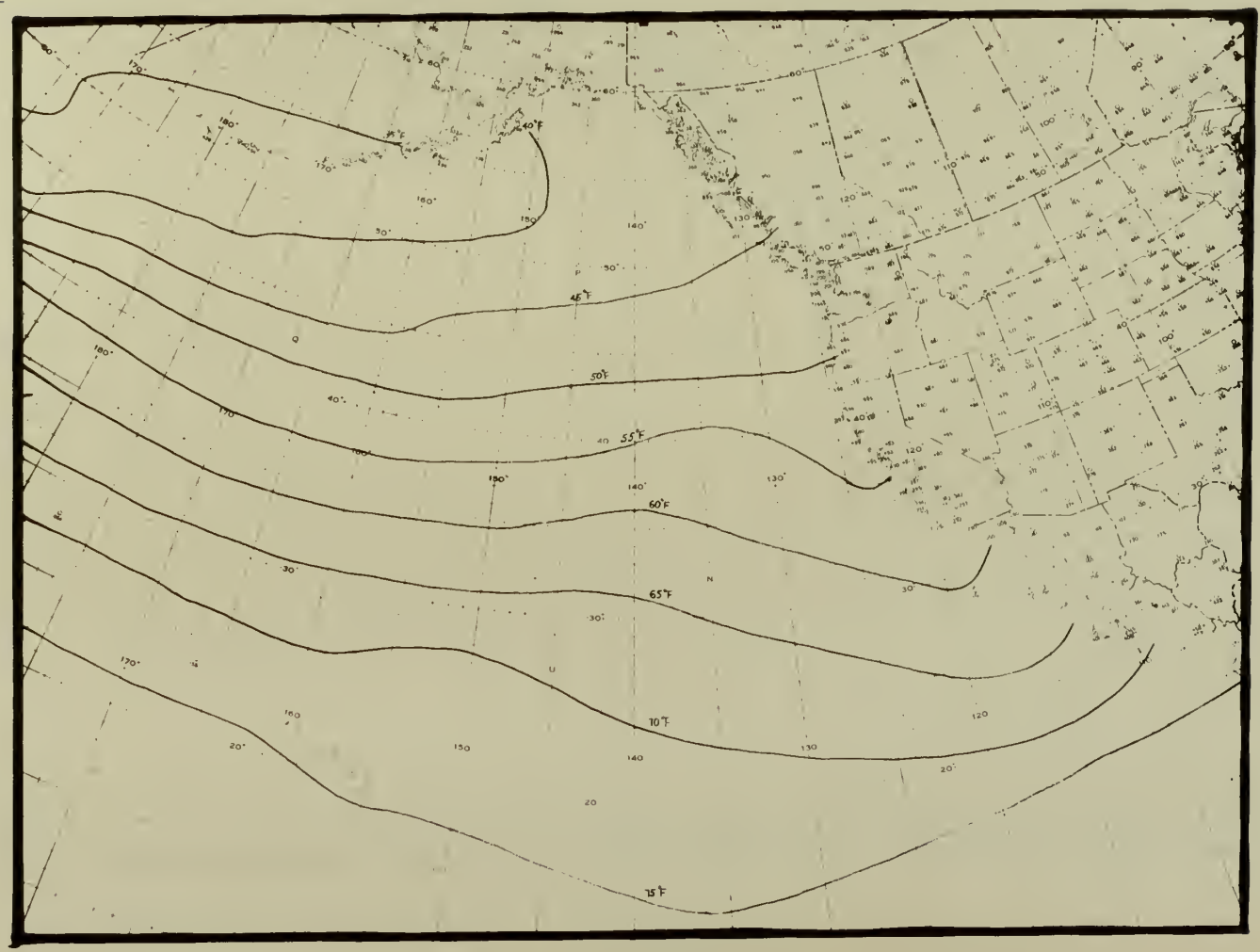

Fig. 17. Mean isotherms of ocean surface water temperature of the month of January.

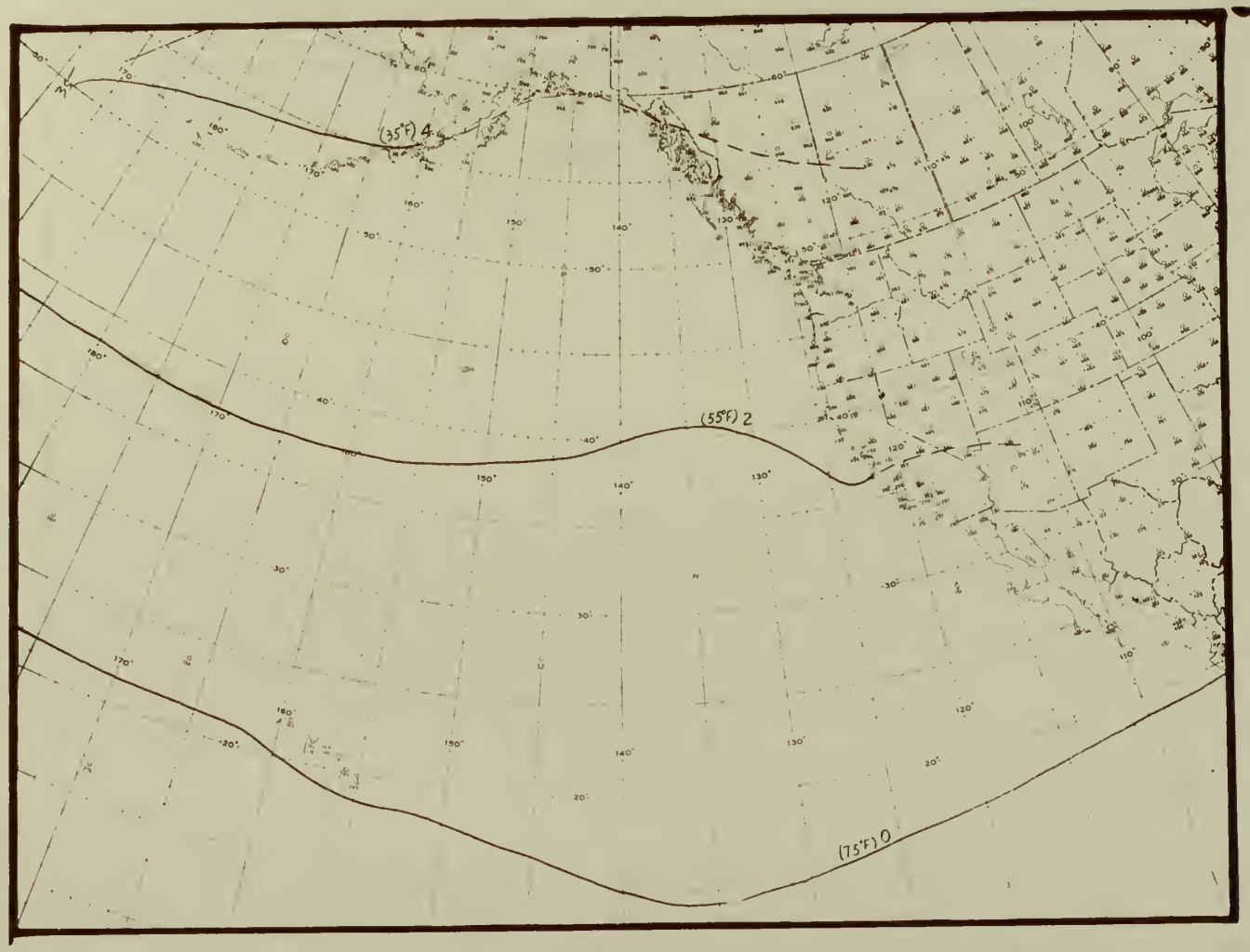

Fig. 18. A chart of function (NT_s) in units of 100 feet. Approximate the coastline of the Gulf of Alaska by an isotherm of 35°F, and set the isotherm of 75°F as zero line for easier manipulation in graphical addition. Note that the $f(NT_s)$ increase as the temperature decreases.

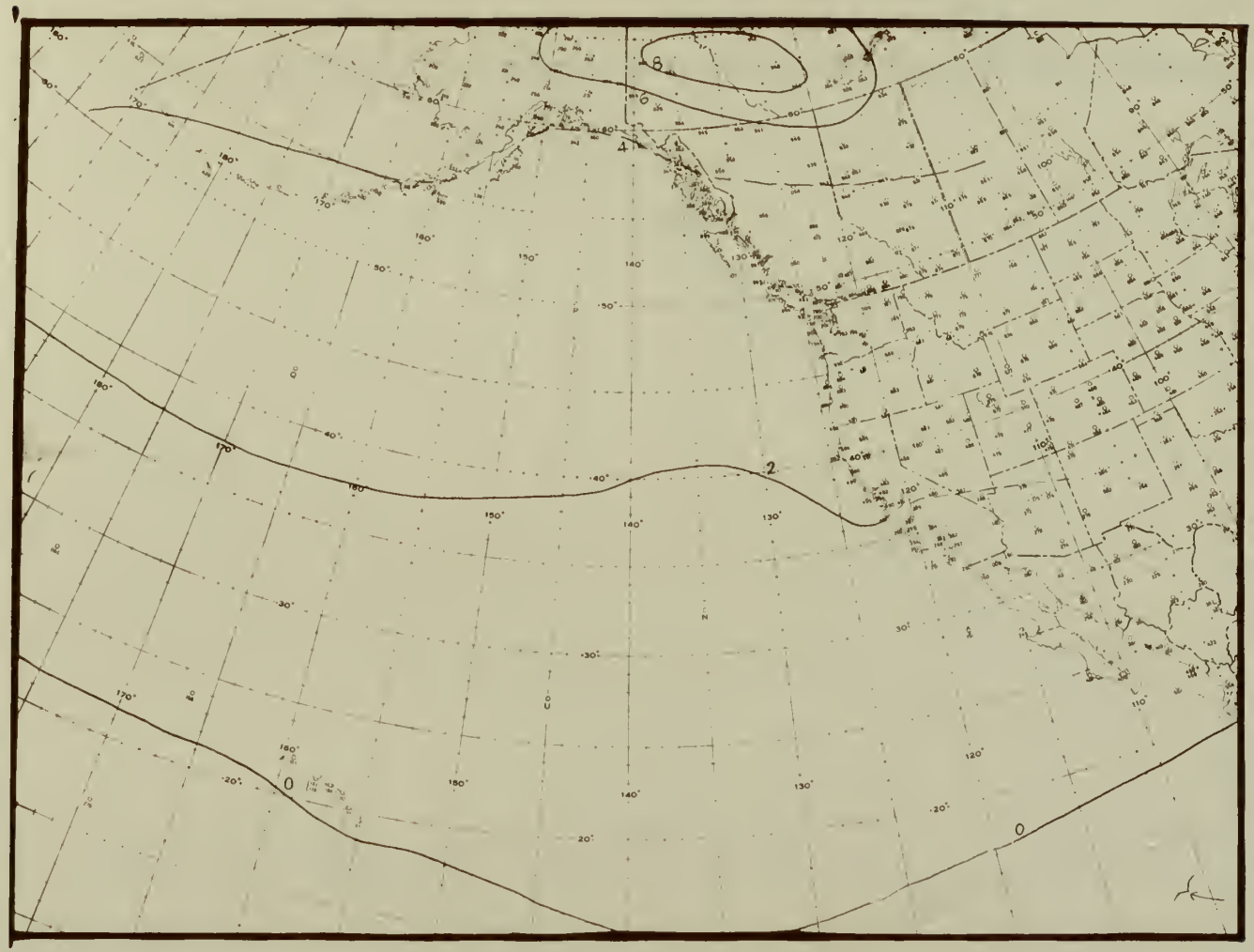

Fig. 19. A chart of function(NT_s) in units of 100 feet included the land area. The f(NT_s) over land is based on the present reported temperature by the land stations at 1500 GMT 4 January

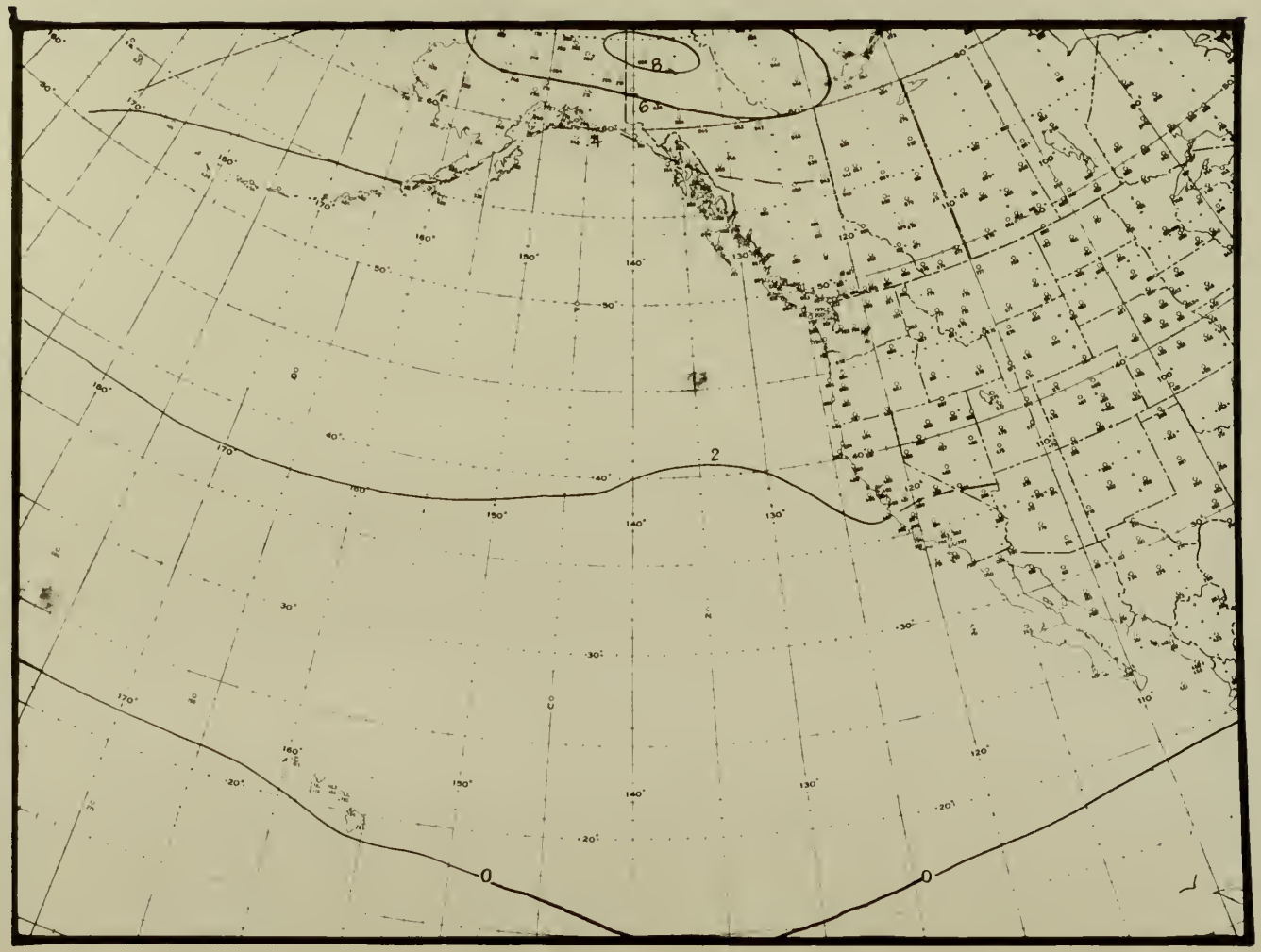

Fig. 20. Function (NI_s) in units of 100 feet included land area prepared at 0000 GMT 6 January 1959 for the prognostication **of the subsequent twelev hours.**

Fig. 21. Function ($N\bar{I}_s$) prepared at 1200 GMT 6 January 1959.

Fig. 22. Function ($N\bar{I}_s$) prepared at 0000 GMT 7 January 1959.

BIBLIOGRAPHY

1. Craddock, J. M., 1951: The warming of arctic air masses over the eastern North Atlantic. Quart. J. r. meteor. Soc., 77, 355-365

2. Fjortoft, R., 1952: On numerical method of integrating the barotropic vorticity equation, Tellus, 4, 179-194.

3. Haltiner. G. J. and Hesse, T. S., 1958: Graphical prognosis including terrain effects. J. meteor., 15, 103-107.

4. Kou, H.-L., 1953: The stability properties and structure of disturbances in a baroclinic atmosphere. J. meteor., 10, 235-243.

5. Reed, R. J., 1958: A graphical prediction Model incorporating a form of non-adiabatic heating. J. meteor., 15, 1-8.

6. Sutcliffe, R. C., 1947: Quart. J. r. meteor. Soc., 77